JOURNAL OF GEOPHYSICAL RESEARCH, VOL. 112, D09109, doi:10.1029/2006JD007461, 2007

Atmospheric volcanic loading derived from bipolar ice cores: Accounting for the spatial distribution of volcanic deposition

Chaochao Gao,[1] Luke Oman,[1,2] Alan Robock,[1] and Georgiy L. Stenchikov[1]

Received 1 May 2006; revised 30 November 2006; accepted 3 December 2006; published 8 May 2007.

[1] Previous studies have used small numbers of ice core records of past volcanism to represent hemispheric or global radiative forcing from volcanic stratospheric aerosols. With the largest-ever assembly of volcanic ice core records and state-of-the-art climate model simulations of volcanic deposition, we now have a unique opportunity to investigate the effects of spatial variations on sulfate deposition and on estimates of atmospheric loading. We have combined 44 ice core records, 25 from the Arctic and 19 from Antarctica, and Goddard Institute for Space Studies ModelE simulations to study the spatial distribution of volcanic sulfate aerosols in the polar ice sheets. We extracted volcanic deposition signals by applying a high-pass loess filter to the time series and examining peaks that exceed twice the 31-year running median absolute deviation. Our results suggest that the distribution of volcanic sulfate aerosol follows the general precipitation pattern in both regions, indicating the important role precipitation has played in affecting the deposition pattern of volcanic aerosols. We found a similar distribution pattern for sulfate aerosols from the 1783–1784 Laki and 1815 Tambora eruptions, as well as for the total β activity after the 1952–1954 low-latitude Northern Hemisphere and 1961–1962 high-latitude Northern Hemisphere atmospheric nuclear weapon tests. This confirms the previous assumption that the transport and deposition of nuclear bomb test debris resemble those of volcanic aerosols. We compare three techniques for estimating stratospheric aerosol loading from ice core data: radioactive deposition from nuclear bomb tests, Pinatubo sulfate deposition in eight Antarctic ice cores, and climate model simulations of volcanic sulfate transport and deposition following the 1783 Laki, 1815 Tambora, 1912 Katmai, and 1991 Pinatubo eruptions. By applying the above calibration factors to the 44 ice core records, we have estimated the stratospheric sulfate aerosol loadings for the largest volcanic eruptions during the last millennium. These loadings agree fairly well with estimates based on radiation, petrology, and model simulations. We also estimate the relative magnitude of sulfate deposition compared with the mean for Greenland and Antarctica for each ice core record, which provides a guideline to evaluate the stratospheric volcanic sulfate aerosol loading calculated from a single or a few ice core records.

Citation: Gao, C., L. Oman, A. Robock, and G. L. Stenchikov (2007), Atmospheric volcanic loading derived from bipolar ice cores: Accounting for the spatial distribution of volcanic deposition, *J. Geophys. Res.*, *112*, D09109, doi:10.1029/2006JD007461.

1. Introduction

[2] Understanding natural causes of climate change is vital to evaluate the relative impacts of human pollution and land surface modification on climate. Of all the natural causes, volcanic eruptions and solar variation are the two most important. *Robock* [2000] reviewed the impacts of volcanism on the Earth's climate system and stressed the need for a reliable record of atmospheric loading of volcanic sulfate aerosols to be able to evaluate the causes of climatic change over the last couple of millennia. Acidity and actual sulfate records from polar firn and ice cores have provided unique details about the nature, timing, and magnitude of volcanic eruptions on regional to global scales. In the last decade, several studies [*Robock and Free*, 1995, 1996; *Zielinski*, 1995; *Clausen et al.*, 1997; *Crowley*, 2000] have used one or a few ice cores to reconstruct the history of explosive volcanism. As more ice cores became available, studies have found large spatial variations in the volcanic sulfate deposition among the Greenland and Antarctic ice cores. For example, the Tambora eruption in 1815 in Indonesia has sulfate fluxes estimated to be between 22.4 kg/km^2 at Plateau Remote [*Cole-Dai et al.*, 2000] and 133 kg/km^2 at Siple Station [*Cole-Dai et al.*, 1997]; the 1783–1784 Laki deposition ranges from 79.7 kg/km^2 at

[1]Department of Environmental Sciences, Rutgers University, New Brunswick, New Jersey, USA.
[2]Now at Department of Earth and Planetary Sciences, Johns Hopkins University, Baltimore, Maryland, USA.

0148-0227/07/2006JD007461$09.00

Humboldt (78.5°N) to 323 kg/km^2 at D3 (69.8°N) [*Mosley-Thompson et al.*, 2003], and from 100 kg/km^2 at North C (74.6°N) to 291 kg/km^2 at Milcent (70.3°N) [*Clausen and Hammer*, 1988]. This large spatial variability raises the question of the reliability of previous reconstructions of atmospheric volcanic sulfate loadings based on a single or only a few ice core records. It also causes problems when comparing the relative magnitudes among different eruptions as well as comparing the same volcanic signal seen in different ice sheets.

[3] The spatial variation of volcanic sulfate deposition may be attributed to site characteristics such as surface irregularity, temperature, wind speed, and surface elevation that can modulate the local accumulation [*Cole-Dai and Mosley-Thompson*, 1999]. The variation may also be caused by local or regional circulation patterns before and during the time of deposition as well as the different deposition mechanisms [*Robock and Free*, 1995]. Estimations based on the average of multiple ice core records can reduce some of the uncertainties [*Robock and Free*, 1995, 1996; *Free and Robock*, 1999; *Mosley-Thompson et al.*, 2003]. However, the number of ice core records decreases as one goes back in time and only a few ice cores are available before 1000 A.D. The uncertainty introduced by the change of ice core availability can be reduced with knowledge of the spatial distribution pattern of volcanic sulfate aerosols.

[4] By measuring the amount of sulfate that was deposited in ice cores, in theory one could do an inverse calculation to estimate the stratospheric loading, and then use this information to calculate the radiative forcing of the climate system [e.g., *Stenchikov et al.*, 1998], one of the ultimate goals of our research. To do this inverse calculation one has to make simplifying assumptions about the area of deposition of the sulfate and the representativeness of deposition on ice for the total atmospheric loading. The simplest assumption would be that sulfate deposition was uniform worldwide, and one could just multiply the mass of sulfate per unit area measured in the ice by the surface area of the Earth (5.1×10^8 km^2). However, our data from Kuwae [*Gao et al.*, 2006] show that the Southern Hemisphere (SH) polar deposition was twice of that of the Northern Hemisphere (NH), suggesting more total deposition in the SH. One could also assume uniform deposition in each hemisphere and that the ice core deposition was representative of the hemispheric average. However, our model simulations, discussed later, show that most deposition occurs at midlatitudes (30°–60°) in each hemisphere, in regions of tropopause folds and strong stratosphere-troposphere transport along the jet stream and storm tracks.

[5] An alternative is to make simplifying assumptions about the transport and deposition of the volcanic sulfate aerosols, and use some reference event to calibrate the stratospheric loading. Several previous studies [e.g., *Clausen and Hammer*, 1988; *Langway et al.*, 1988; *Zielinski*, 1995] used factors derived from observations of radioactivity from nuclear bomb tests to estimate stratospheric sulfate loading, assuming a similar global distribution pattern between the radioactivity from bomb tests and sulfate injected into the atmosphere by violent volcanic events. Other studies [e.g., *Cole-Dai and Mosley-Thompson*, 1999] assumed a similar global transport pattern for all of the low-latitude eruptions and used the observed aerosol loading of the Pinatubo eruption and its deposition in six South Pole ice cores to calibrate atmospheric loadings of other low-latitude eruptions. However, *Zielinski* [1995] found that the atmospheric loadings derived in the first group of studies were 2–5 times larger than those calculated from stratospheric observations for recent eruptions by *Sato et al.* [1993]. The radioactivity data used in these studies was based on the United Nations Scientific Committee on the Effects of Atomic Radiation (UNSCEAR) 1982 Report [*UNSCEAR*, 1982] which used the total atmospheric loading rather than the stratospheric portion. The up-to-date UNSCEAR 2000 Report [*UNSCEAR*, 2000] includes new information that was previously unavailable and it separates the stratosphere from the troposphere. In this study, we recalculate the calibration factors using the 2000 Report. In the second group of studies the calibration was only done for the South Pole ice cores and the result may be very different for ice cores in other regions. In addition, the hemispheric partitioning of volcanic clouds could be quite different than that for the Pinatubo eruption, depending on the location of the eruption, height of the plume, location of the Intertropical Convergence Zone, phase of the Quasi-Biennial Oscillation, and stratospheric winds when the eruption took place. Sulfate deposition records from both polar ice cores can help us to determine the hemispheric partitioning of these volcanic events.

[6] In the present study, we have incorporated the volcanic signals derived from 44 ice cores records, 24 from Greenland plus one from Mt. Logan and 19 from Antarctica, together with NASA Goddard Institute for Space Studies (GISS) ModelE climate model simulations to estimate the spatial distribution of volcanic sulfate aerosols in Greenland and Antarctic ice sheets and the stratospheric mass loading of the largest volcanic eruptions in the past 1000 years. This paper is organized as follows: Section 2 describes the ice core database and the methods to extract the volcanic signals and calculate the sulfate deposition, section 3 summarizes the spatial aerosol distribution patterns of the largest volcanic eruptions on the Greenland and Antarctica ice sheets and their comparison with those simulated by ModelE coupled to a sulfate chemistry model, and calculations of stratospheric loadings for these eruptions using new knowledge derived from bomb tests and model results are given in section 4. As this model explicitly simulates the stratospheric volcanic loading, although imperfectly, comparisons with the observations give important constraints on the validity of both the model and the observations. Discussion and conclusions are presented in section 5. This is the first study to use ice core records to investigate the spatial distribution patterns of volcanic sulfate on regional to continental scales. Our results not only provide a guideline to reconstruct a long-term volcanic forcing index with a reduced body of ice core records, but also serve as a reference to evaluate model simulations of volcanic deposition.

2. Ice Core Database and Volcanic Deposition Calculation Methodology

[7] We have selected seven major low-latitude eruptions during the last millennium, Unknown (1259), Kuwae (1452

Table 1. Ice Core Time Series Used in the Study[a]

Name	Location	Period	Resolution	Measure Type	Units	Reference
NGT_B20	79°N, 36.5°W	830–1993	12/yr	CFA	ng/g (ppb)	*Bigler et al.* [2002]
NorthGRIP1	75.1°N, 42.3°W	190–1969	1/yr	total SO_4	μequiv./kg	*Gao et al.* [2006]
GISP2[b]	72.6°N, 38.5°W	1–1984	0.5/yr	NSS SO_4	ppb	*Zielinski* [1995]
Greenland Site T	72.6°N,38.5°W	1731–1989	1/yr	EXS	kg/km^2	*Mosley-Thompson et al.* [1993]
Greenland Site A	70.8°N, 36°W	1715–1985	1/yr	EXS	kg/km^2	*Mosley-Thompson et al.* [1993]
20D[b]	65°N, 45°W	1767–1983	1/yr	NSS SO_4	ng/g	*Mayewski et al.* [1990]
Mt. Logan[b]	60.6°N,140.6°W	1689–1979	1/yr	total SO_4	μequiv./l	*Mayewski et al.* [1993]
Law Dome	66.7°S 112.8°E	1301–1995	12/yr	NSS SO_4	μequiv./l	*Palmer et al.* [2002]
Dyer	70.7°S, 65°W	1505–1989	1/yr	total SO_4 flux	kg/km^2	*Cole-Dai et al.* [1997]
G15[b]	71.2°S, 46°E	1210–1983	varies	DEP	μS/m	*Moore et al.* [1991]
Talos Dome	72.8°S, 159.1°E	1217–1996	varies	NSS SO_4	μequiv./l	*Stenni et al.* [2002]
Hercules Névé	73.1°S, 165.5°E	1774–1992	1/yr	NSS SO_4	μequiv./l	*Stenni et al.* [1999]
Dome C[b]	74.7°S, 124.2°E	1763–1973	1/yr	NSS SO_4	μequiv./l	*Legrand and Delmas* [1987]
DML_B32	75°S, 0°W	159–1997	varies	NSS SO_4	ng/g	*Traufetter et al.* [2004]
Siple Station	76°S, 84.3°W	1417–1983	1/yr	Total SO_4 flux	kg/km^2	*Cole-Dai et al.* [1997]
ITASE 01-5	77°S, 89°W	1781–2002	varies	SO_4	μg/l	*Dixon et al.* [2004]
ITASE 00-5	77.7°S, 124°W	1708–2001	varies	SO_4	μg/l	*Dixon et al.* [2004]
ITASE 00-4	78°S, 120°W	1799–2001	varies	SO_4	μg/l	*Dixon et al.* [2004]
ITASE 01-3	78.1°S, 95.6°W	1859–2002	varies	SO_4	μg/l	*Dixon et al.* [2004]
ITASE 00-1	79.4°S, 111°W	1651–2001	varies	SO_4	μg/l	*Dixon et al.* [2004]
ITASE 99-1	80.6°S,122.6°W	1713–2000	varies	SO_4	μg/l	*Dixon et al.* [2004]
Plateau Remote[b]	84°S, 43°E	1–1986	1/yr	SO_4	ppb	*Cole-Dai et al.* [2000]
PS1[b]	90°S	1010–1984	1/yr	NSS SO_4	ng/g	*Delmas et al.* [1992]
PS14[b]	90°S	1800–1984	1/yr	NSS SO_4	ng/g	*Delmas et al.* [1992]
SP2001 (core 1)	90°S	905–1999	1/yr	Total SO_4 flux	kg/km^2	*Budner and Cole-Dai* [2003]
SP95	90°S	1487–1992	varies	SO_4	μg/l	*Dixon et al.* [2004]

[a]DEP, dielectric profiling; NSS SO_4, non-sea-salt sulfate; CFA, continuous flow analysis; EXS, excess sulfate. Note that ng/g = μg/kg = μg/l = ppb.
[b]Cores used by *Robock and Free* [1995].

or 1453), Unknown (1809), Tambora (1815), Krakatau (1883), Agung (1963), and Pinatubo (1991), to study the spatial pattern of the volcanic sulfate deposition in the ice cores. These events were chosen because all of them are large explosive volcanic eruptions (Volcanic Explosivity Index $\geq$5) [*Newhall and Self*, 1982] that have signals in almost every available ice core record. In Greenland, we only have six ice cores with original sulfate data and among the six cores only three go back before 1500 A.D. We thus decided to use the 1809 Unknown, Tambora, and Krakatau eruptions as examples for low-latitude eruptions and added Laki and Katmai (1912) to represent high-latitude eruptions. *Mosley-Thompson et al.* [2003] calculated the sulfate deposition for Laki and Tambora for six PARCA (Program for Arctic Regional Climate Assessment) ice cores; *Clausen and Hammer* [1988] (hereinafter referred to as CH88) also computed the deposition for the same two eruptions for 12 Greenland ice cores. We combined these two analyses with our ice core results to obtain a more comprehensive understanding of the spatial pattern in Greenland ice cores. Table 1 lists general information and references for the 26 ice core records analyzed in this study. Information about the six PARCA and 12 CH88 Greenland ice cores can be found in the work by *Mosley-Thompson et al.* [2003] and *Clausen and Hammer* [1988], respectively. For our 26 records we first extracted volcanic deposition signals by applying a high-pass loess filter to the time series and examining peaks that exceed twice the 31-year running median absolute deviation [*Gao et al.*, 2006]. Then we evaluated the sulfate fluxes for the above nine events from the 26 cores and adjusted the timing of the signals so that the peak deposition of each event corresponds to the same year. After that, we calculated the total deposition for each eruption in the individual ice core by summing the deposition in the years that follow the eruption. The resulting sulfate deposition, together with those from six PARCA and 12 CH88 records, was plotted for individual eruptions.

3. Spatial Distribution of Volcanic Sulfate Deposition

3.1. Greenland Ice Cores

[8] Figure 1 shows the spatial distributions of the Laki, 1809 Unknown, Tambora and Krakatau volcanic sulfate deposition in the Greenland ice cores; Figure 2 shows the spatial patterns of the deposition interpolated into 0.5° $\times$ 0.5° grid points. The interpolation was done using a *Cressman* [1959] objective analysis on the station data to yield a gridded result representing the station data. From Figures 1 and 2 we see that despite some local variations among the ice cores there are some common spatial patterns at a regional scale, which generally follows the pattern of annual total precipitation (solid + liquid) [*Box et al.*, 2004, Figure 6]. For example, there is above average deposition along the intermediate elevations on the western slope with the maximum located near 70°N, below average deposition on the northeast side of the Greenland ice divide with minima found in the interior area of northern Greenland, and large deposition on the west coast of north Greenland above Melville Bay. We found a positive linear correlation between volcanic deposition and annual accumulation rate at the 95% confidence level for three (Laki, 1809 Unknown,

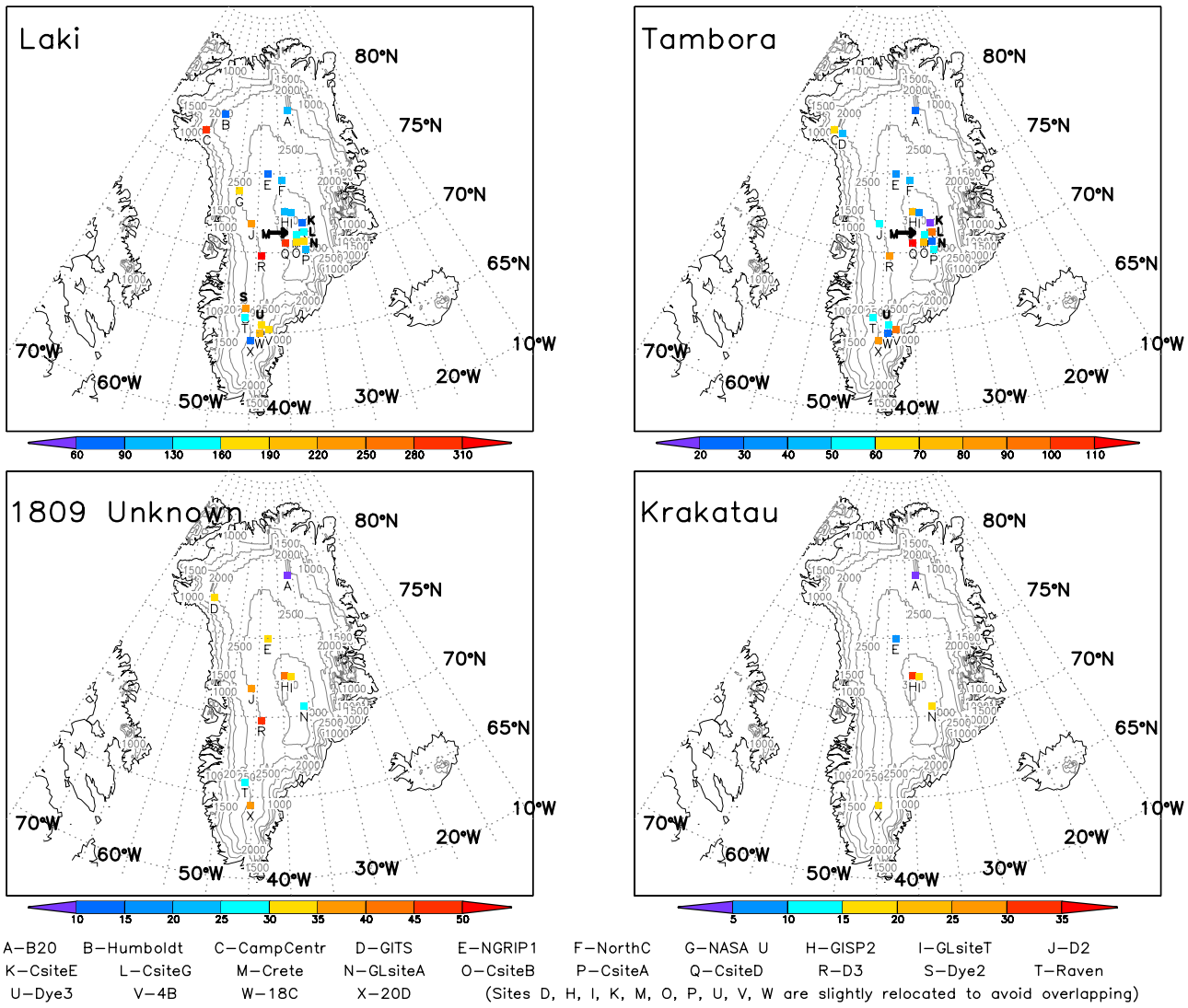

Figure 1. Spatial distribution of Laki, 1809 Unknown, Tambora, and Krakatau sulfate deposition (kg/km^2) in Greenland ice cores. The colors are defined so that blue indicates smaller than average deposition and yellow, orange, and red indicate larger than average.

and Tambora) of the four eruptions (Figure 3). The smaller significance in the case of the Krakatau eruption (89%) was due to the small number of data points available. This correlation between volcanic deposition and annual accumulation rate is in agreement with the results of *Legrand and Delmas* [1987] and *Mosley-Thompson et al.* [2003], which indicates that the sulfate aerosols are more or less homogeneous in the atmosphere and the deposition in the ice sheet depends on the accumulation rates. No significant difference at regional scale was found between the spatial distribution of the Laki and Tambora fallouts, which implies that the deposition mechanism is probably the same for the low-latitude and high-latitude eruptions in Greenland.

[9] From Figures 1 and 2 we can also see that ice cores in northern Greenland (>72°N) usually have less than average volcanic deposition, except for the ones on the west coast. Thus volcanic stratospheric loadings based only on northern Greenland ice core records (e.g., B20, Humboldt, North-GRIP1, and North Central) may very likely have been underestimated. The ice cores located at elevation 2000–2500 m on the west slope of the ice sheet (e.g., NASA-U, D2, and D3) usually receive larger than average deposition, probably caused by precipitation enhancement due to orographic lifting. Maximum deposition was found in the cores located between 40°W and 45°W near 70°N, such as Crête sites B and D. Stratospheric aerosol mass loadings derived only from these cores may thus have been overestimated.

[10] Larger spatial variations exist in deposition in the ice cores across Greenland, and the amplitude of this variability varies among different eruptions. For example, the spatial variability (defined as the ratio between the spatial standard deviation of sulfate deposition and the mean deposition) changes from 34–46% for high-latitude eruptions such as Katmai and Laki, to 41–48% for big low-latitude eruptions such as 1809 Unknown and Tambora, and further to 61–129% for smaller equatorial eruptions such as Krakatau and Agung. We also found that increasing the number of ice cores did not necessarily reduce the spatial variability. For instance, the variation of Laki and Tambora was larger than that of Katmai and 1809 Unknown although

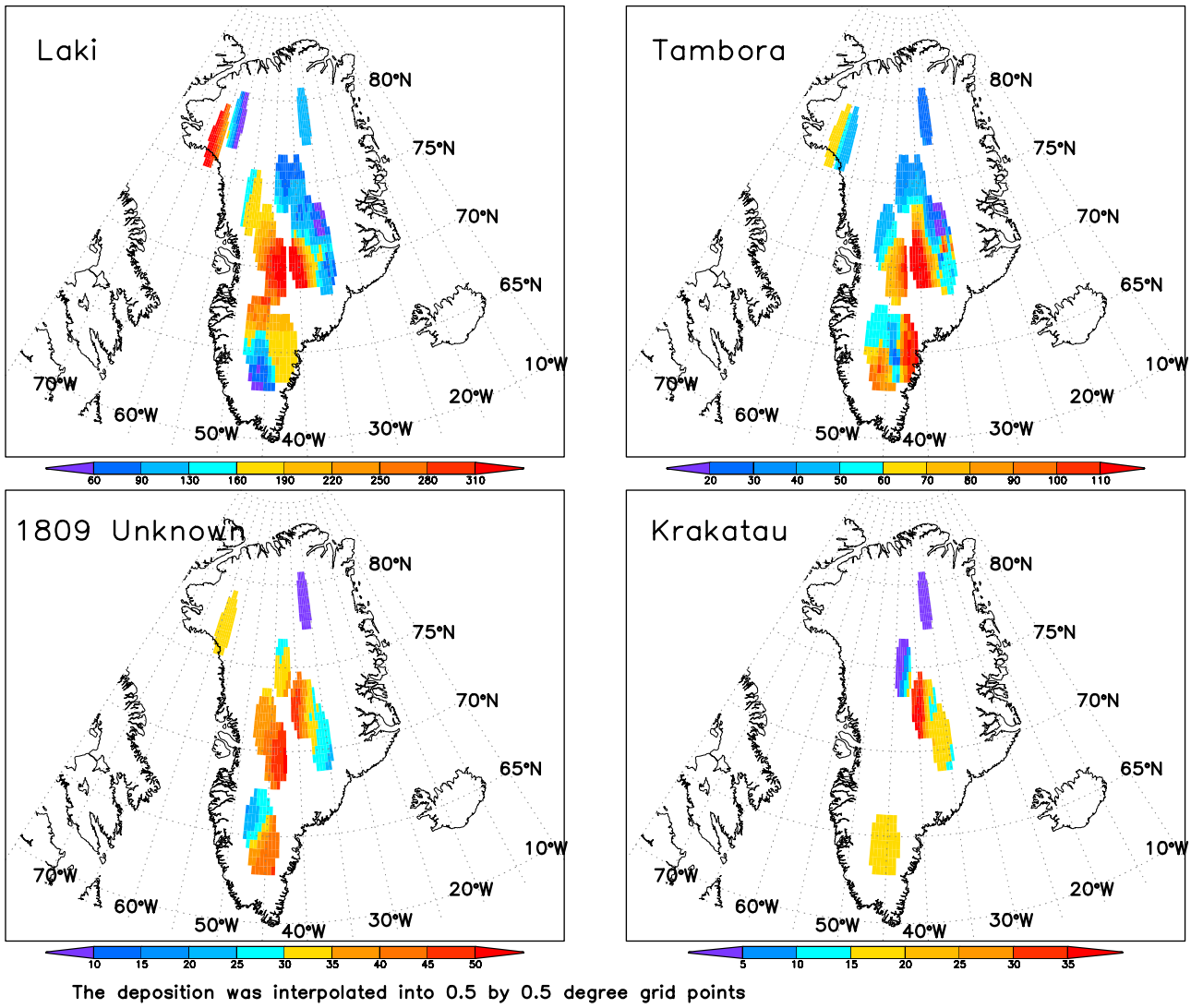

Figure 2. Same as Figure 1 but with the deposition interpolated into 0.5° × 0.5° grid points.

the number of cores available for Laki and Tambora was four times and twice as large as Katmai and 1809 Unknown, respectively. Spatial variability of the same or larger magnitude also exists at local scale. In the summit region of central Greenland we found a decrease of 53% from Crête site D to Crête in the volcanic sulfate aerosol deposition for the Laki eruption and 55% for Tambora, and a further decrease of 60% across the ice divide from Crête to Crête site E for Laki and 75% for Tambora. *Clausen et al.* [1988] also found that site E is located in an accumulation "shadow" area compared to the corresponding region east of the ice divide.

3.2. Antarctic Ice Cores

[11] Figure 4 shows the spatial distributions of sulfate deposition for the 1809 Unknown, Tambora, Krakatau, and Agung eruptions respectively in the Antarctic ice cores. From Figure 4 we can see a distribution pattern that is similar in regional scale for all of the four events: large deposition over the Antarctic Peninsula, West Antarctica and along the coast of East Antarctica; and small values over the plateau of East Antarctic and around Dronning Maud Land and Victoria Land. This pattern is generally in agreement with the long-term accumulation distribution in Antarctica [*Bromwich et al.*, 2004, Figure 2]. In the case of individual ice cores, Siple Station always has the highest deposition, followed by Dyer and the ITASE cores, all located in West Antarctica. *Reusch et al.* [1999] and *Dixon et al.* [2004] found that West Antarctica is the most stormy area of the continent, affected by several large atmospheric low-pressure systems, the Amundsen Sea Low, the Weddell Sea Low and the Davis Sea Low, which serve as the primary transport mechanisms for moisture and aerosols to the West Antarctic ice sheet. This leads to more precipitation and therefore more sulfate deposition in West Antarctica. The deposition at the four South Pole cores is relatively stable and is close to the continental averages. Law Dome usually has higher than average deposition. Plateau Remote, Dome C, DML-B32, Talos Dome and Hercules Névé always have lower than average deposition. Among the five sites, Plateau Remote and Dome C are located in one of the lowest long-term accumulation zones, with annual precipitation accumulation less than 50 mm/yr and elevation above

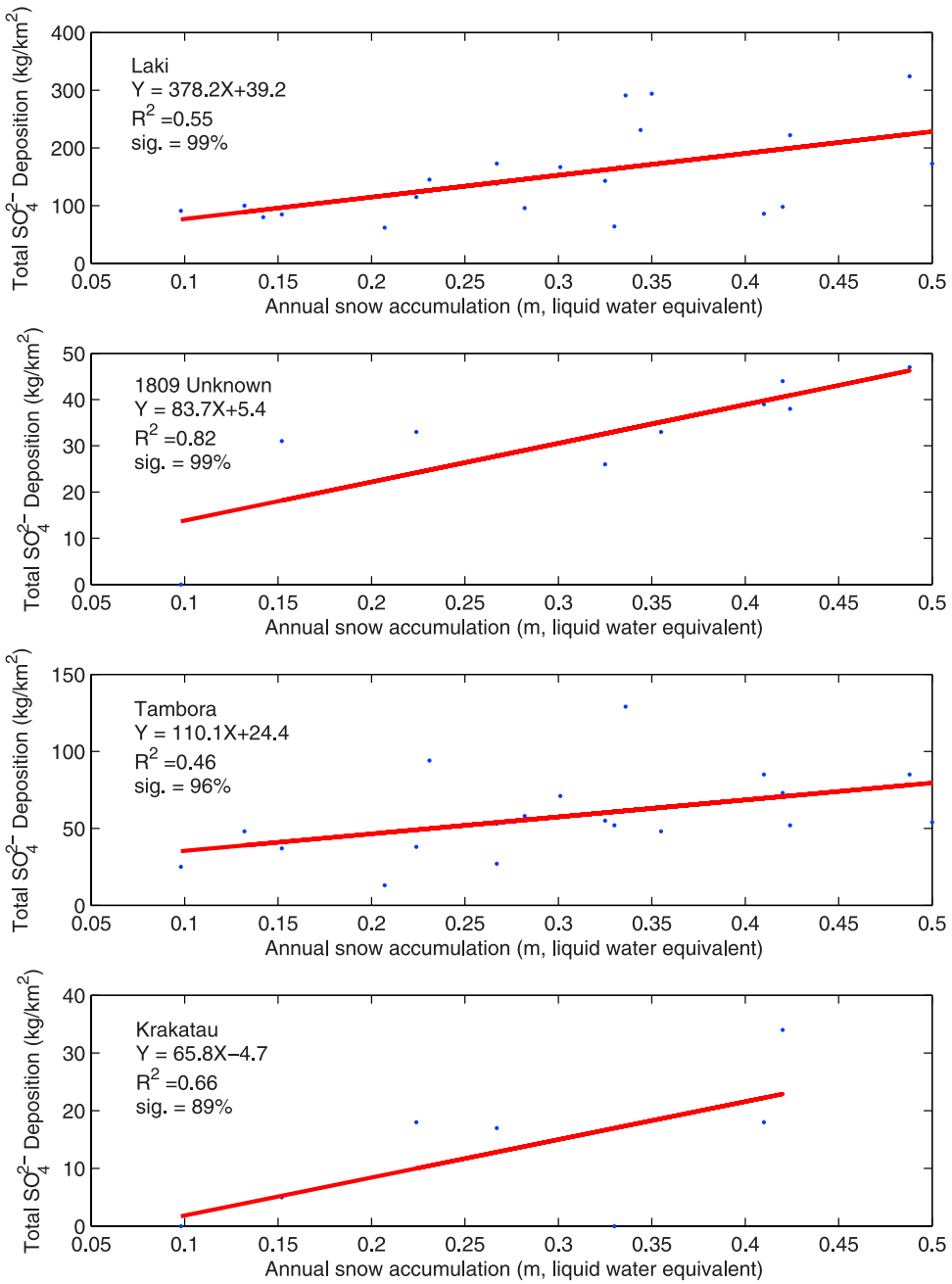

Figure 3. Relationship between the annual snow accumulation rates and the total sulfate fluxes in Greenland ice cores.

3000 km. These two cores also have the lowest correlation coefficients with the other sites, which indicates that the volcanic deposition in these sites is not representative of other regions of Antarctica and vice versa. *Cole-Dai et al.* [1997] found the important role of postdepositional redistribution in regulating the volcanic signals in Plateau Remote. On the other hand, Plateau Remote and DML_B32 are the only two among these 19 cores that have records during 0–1000 A.D. Proper adjustment is thus needed to account for the spatial difference when using these two records to construct volcanic forcing time series for the early periods.

[12] Figure 5 shows the spatial distribution of sulfate deposition for the 1259 Unknown, Kuwae, and Pinatubo eruptions. Although the numbers of ice core records available for these events are smaller than those for the previous four events, the spatial patterns of volcanic sulfate deposition are generally in agreement. The only exceptions are the larger-than-average deposition in Plateau Remote and Talos Dome for the Kuwae eruption. The reasons for these departures of volcanic sulfate deposition from the general pattern are yet to be investigated. It might have been caused by postredistribution of the volcanic deposition or by different weather conditions, such as the circulation pattern at the time when the volcanic debris was deposited on the

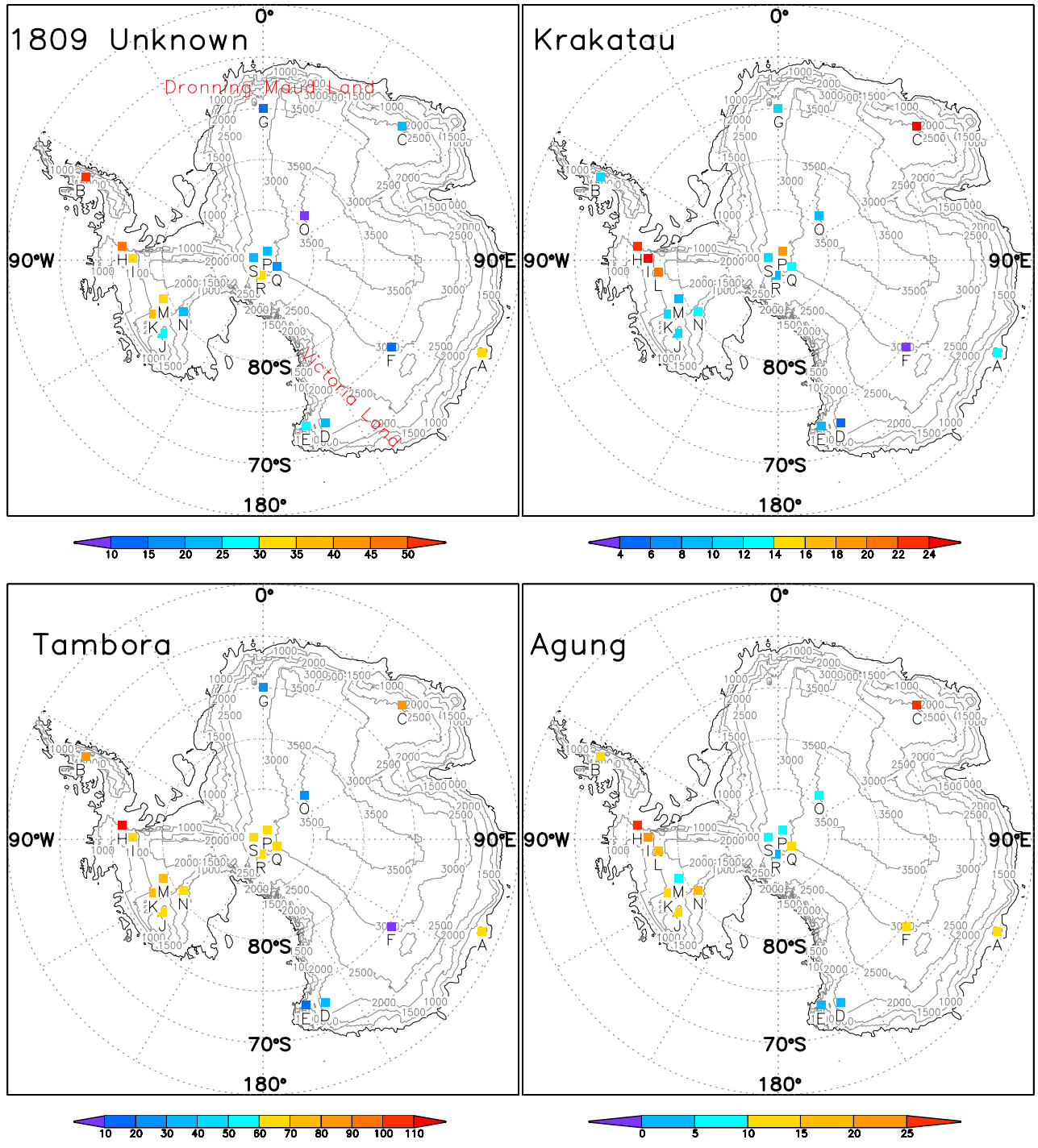

Figure 4. Spatial distribution of 1809 Unknown, Tambora, Krakatau, and Agung sulfate deposition (kg/km^2) in Antarctic ice cores. The colors are defined so that blue indicates smaller than average deposition and yellow, orange, and red indicate larger than average.

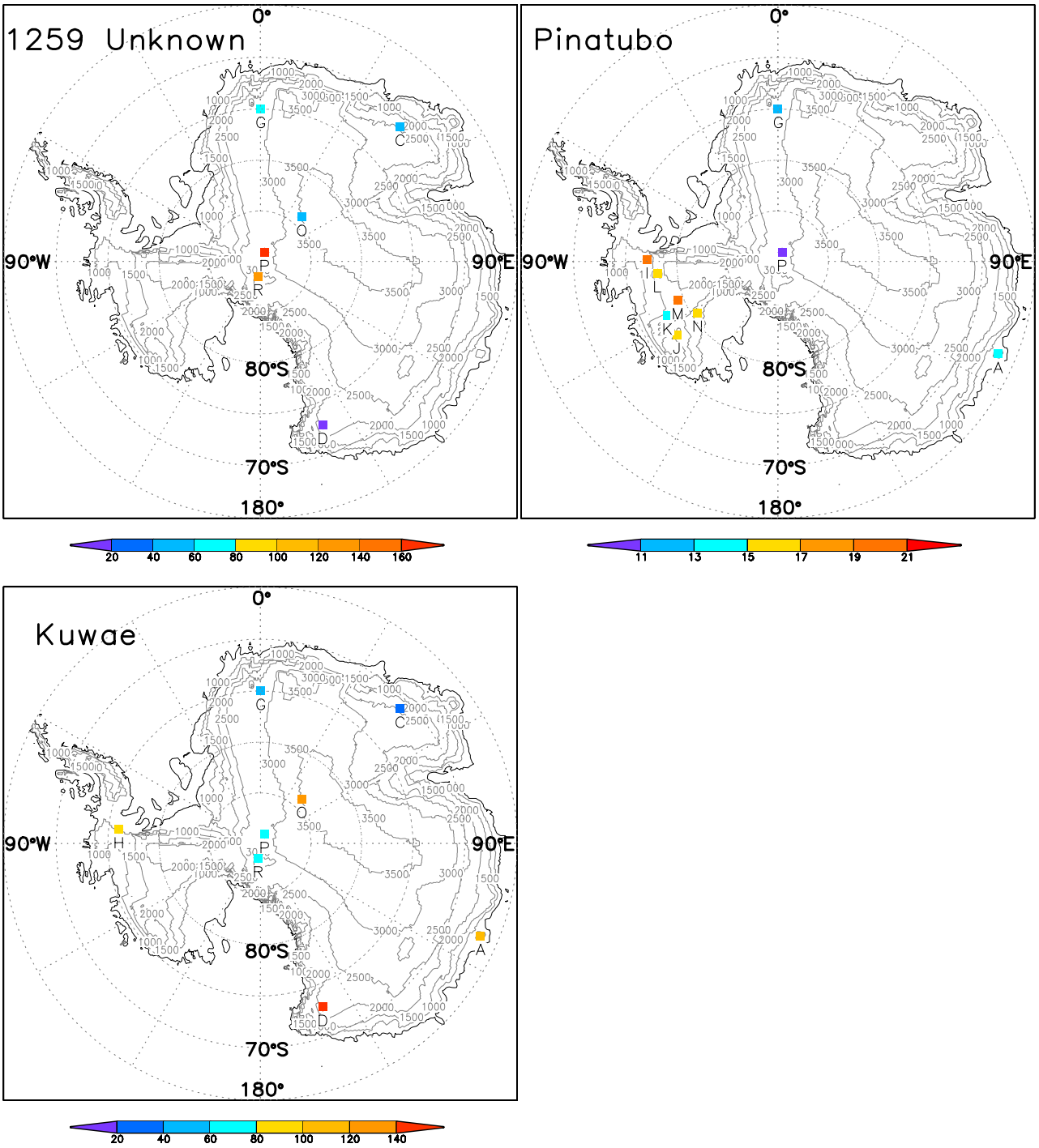

Figure 5. Same as Figure 4 but for the 1259 Unknown, Kuwae, and Pinatubo eruptions.

Antarctic ice sheet. Similar to the Greenland ice cores, we found a spatial variability of 44% and 48% for the 1809 Unknown and Tambora eruption separately across the Antarctic ice cores. The variability increased to 49%, 54%, and 65% for the moderate eruptions as Krakatau, Pinatubo, and Agung eruption respectively.

[13] In summary, we found that despite some local variability in Greenland and a few discrepancies in Antarctica, the volcanic sulfate deposition obtained from these 24 Greenland (six in Table 1, six PARCA, and 12 CH88), one Mt. Logan, and 19 Antarctic (Table 1) ice cores displays consistent spatial distribution patterns that resemble the general pattern of annual precipitation accumulation rates in Greenland and Antarctica, respectively. This indicates that the volcanic debris is more or less evenly distributed in the atmosphere before it reaches the surface. We also found that deposition in most of the individual ice cores is consistent in its ratio to the Greenland or Antarctica mean deposition for all of the eruptions listed in this paper, being consistently smaller or larger. On the other hand, spatial variability of about 45% was found for sulfate deposition across both the Greenland and Antarctic ice cores for large eruptions such as Tambora and 1809 Unknown, and this variability increases substantially for moderate eruptions such as Pinatubo and Agung because of lower mean deposition. We also found site to site variations as large as a factor of four among nearby ice cores in Greenland. Therefore it is important to obtain good spatial coverage of ice cores from different geographical areas to accurately estimate atmospheric volcanic sulfate loading. Most of the currently available ice core records are concentrated in the areas of central Greenland, central South Greenland, West Antarctica, and the South Pole. Future studies using ice core records may benefit from new cores drilled in other regions. For the early periods, when there are only a few cores available from certain regions, the total volcanic deposition should be carefully adjusted according to their ratios to the Greenland or Antarctica mean [*Gao et al.*, 2006]. Finally, although the volcanic sulfate deposition presented here for Greenland is from three different studies that used three different methods to extract the volcanic peaks, the results should be robust because for volcanic eruptions as large as Laki, 1809 Unknown, and Tambora, the background variation should not affect the extraction of peaks and calculation of volcanic deposition no matter what method was used.

3.3. Comparison With GISS ModelE Simulations

[14] Simulations were conducted of the volcanic aerosol transformation and distribution following the Pinatubo, Tambora, Katmai, and Laki eruptions using the GISS ModelE general circulation model coupled to a sulfur chemistry module [*Oman et al.*, 2006]. This particular version of the model has $4^\circ \times 5^\circ$ horizontal resolution and 23 vertical levels. The model has both dry and wet deposition schemes coupled to climate model processes [*Koch et al.*, 2006]. A complete description of the model is given by *Schmidt et al.* [2006]. Several ensemble runs were conducted for each of these eruptions, and the results used here were the ensemble averages. Approximately 10–20% differences in sulfate deposition over Greenland and Antarctica were found between individual ensemble runs. We injected the following amounts of SO_2 gas for each eruption: 20 Mt for Pinatubo, 55 Mt for Tambora, 5 Mt for Katmai, and 122 Mt for Laki.

[15] Because of the coarse horizontal resolution, the model cannot capture details of local, small-scale variations of sulfate deposition. However, at regional and continental scales the model produced spatial patterns similar to those from ice core observations. Figure 6 shows the model-simulated volcanic sulfate deposition in both Greenland and Antarctica and their corresponding ice core observations for the Tambora eruption. The model produces low deposition along the east side of the ice divide as well as for interior Northern Greenland, and high deposition in the West and Central Greenland and coastal regions. Over Antarctica it produces high deposition in West Antarctica and low deposition in the east Plateau region. Different from the ice core observations, the highest deposition in the model is found to be over the Transantarctic Mountains. All of the four ModelE eruptions produce a similar deposition pattern in Greenland, as well as for the overall Arctic region (Figure 7). Similar deposition patterns were also found among individual ensemble runs. This similarity indicates that the initial weather conditions play a relatively minor role in the ultimate sulfate deposition pattern. The spatial variation across both Antarctica and Greenland is also found to be mostly explained by variations in the precipitation rate across these regions. On the other hand, the average deposition over the grid points where we have ice core measurements is as much as twice as large as that of ice core observations for Tambora (58.3 kg/km^2 versus 78.4 kg/km^2 in Greenland, 58.8 kg/km^2 versus 113.3 kg/km^2 in Antarctica). The difference in the magnitude of sulfate deposition between the model simulation and ice core observations could be caused by the difference in the initial injection of sulfur dioxide gas, the SO_2 to SO_4 conversion efficiency, the hemispheric partitioning of volcanic clouds, and the transport speed and pathways of the sulfate aerosols between the model realization and what actually happened during each eruption. Furthermore, the model's coarse resolution and smooth topography may hinder its capability to accurately simulate the deposition; and its lack of a proper simulation of the Quasi-Biennual Oscillation may cause a noticeable impact on the aerosol distribution for low-latitude eruptions [*Hitchman et al.*, 1994; *Haynes and Shuckburgh*, 2000].

4. Estimation of Stratospheric Volcanic Sulfate Loading

[16] With the volcanic sulfate records from the ice cores, we can do an inverse calculation of the stratospheric aerosol loading for each individual eruption. This information can then be used to calculate the radiative forcing of the climate system, one of the ultimate goals of our research. To do this calculation, we first calculated the average volcanic sulfate deposition in the two ice caps. Then we reexamined the bomb test calculations using the up-to-date *UNSCEAR* [2000] report and updated the Pinatubo-based calibration factor using our extended assembly of ice core observations. After that we calculated another set of calibration factors using the *Oman et al.* [2006] coupled chemistry/climate model simulations and evaluated the sensitivity of these

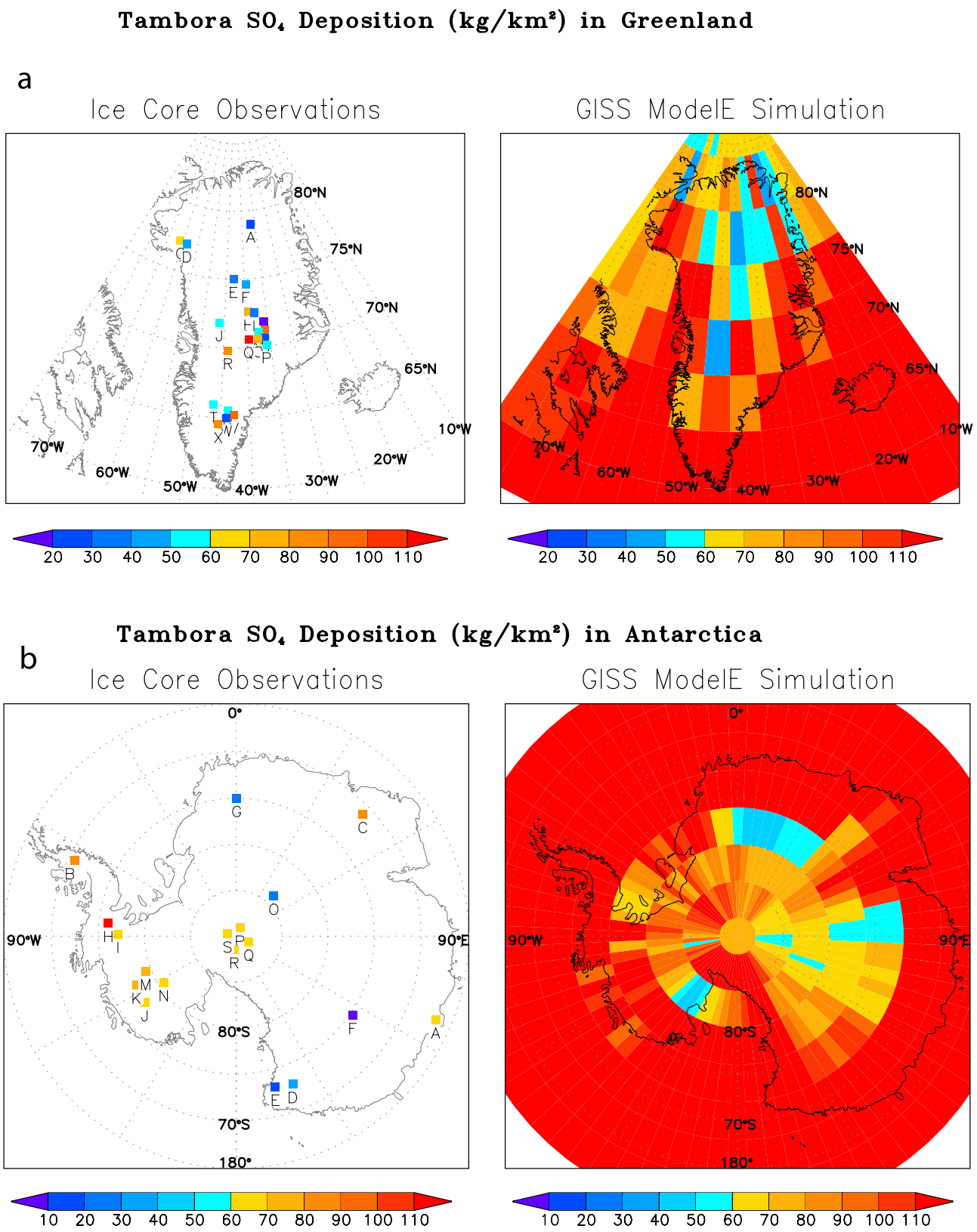

Figure 6. Comparison between the total Tambora sulfate deposition (kg/km^2) in (top) Greenland and (bottom) Antarctic ice core observations and in the GISS simulations.

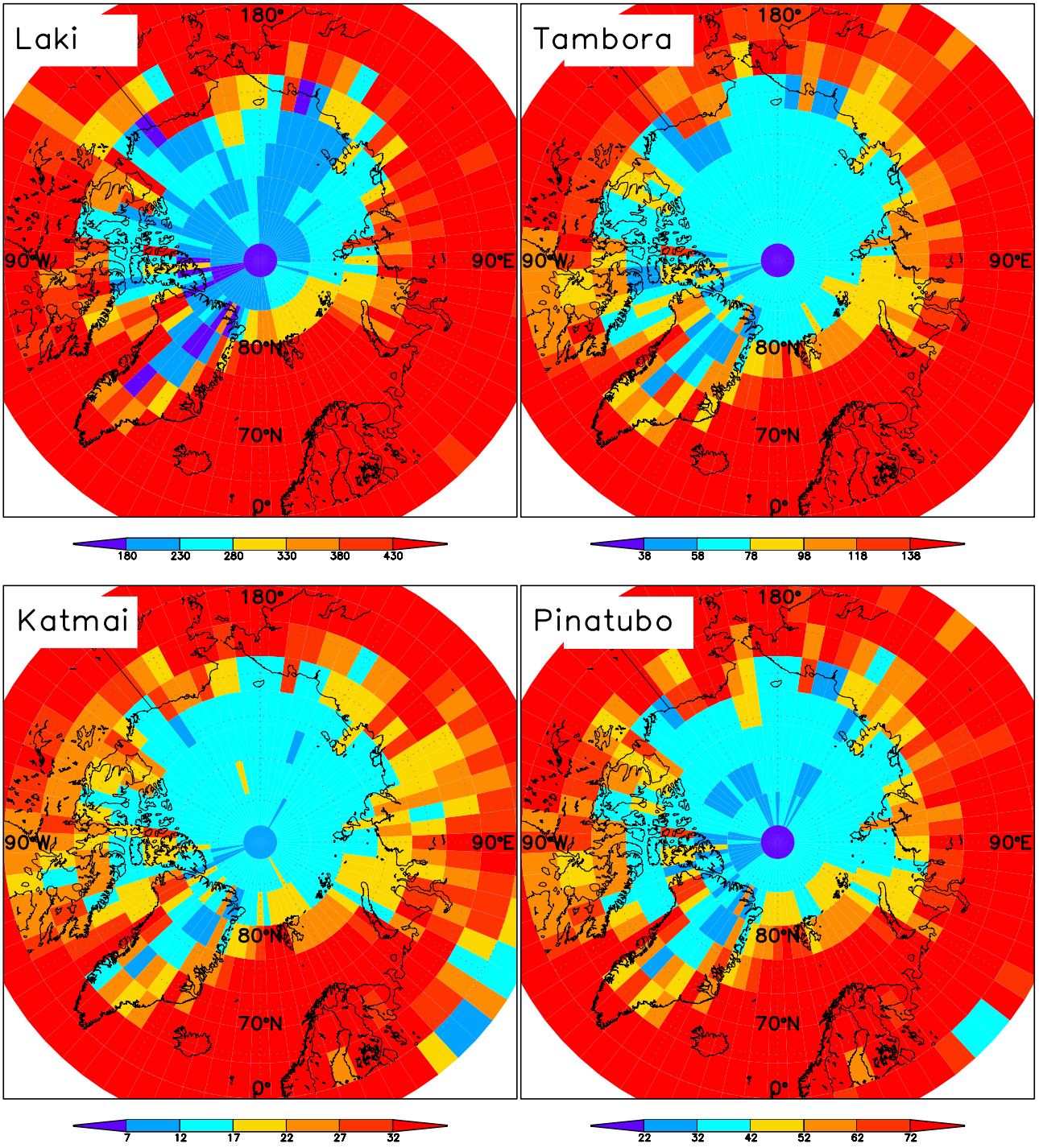

Figure 7. GISS simulated Laki, Katmai, Tambora, and Pinatubo deposition (kg/km^2) in the Arctic region. The colors are defined so blue indicates smaller than average deposition for 66°N–82°N, 50°W–35°W and yellow, orange, and red indicate larger than average.

calibration factors among the different methods. Finally we calculated the stratospheric loadings of the large volcanic eruptions during the past 1000 years by applying these factors to the 44 ice core records.

4.1. Calculation of the Greenland and Antarctic Mean Volcanic Sulfate Deposition

[17] From Figures 1 and 4 we can see that the ice cores are not evenly distributed in either Greenland or Antarctica. To account for this spatial difference in ice core distribution, we first calculated the local average deposition for each area where there are at least two ice cores drilled close by. For example, in calculating the Tambora deposition in the Arctic we first calculated the average deposition in central Greenland, southern Greenland, and the northwest coast (i.e., average of Camp Century and GITS) of Greenland. Then we combined these local averages with the deposition from other ice cores, including Mt. Logan, to calculate the

Table 2. Estimates of Stratospheric Sulfate Loading From Large Explosive Volcanic Eruptions

Eruption	Year	Number of Cores Used in Average	Ice Core Average Sulfate Deposition, kg/km^2	Calibration Factor, $\times 10^9$ km^2	Hemispheric Stratospheric Sulfate Aerosol Loading, Tg	Global Stratospheric Sulfate Aerosol Loading, Tg
Unknown	1259	NH (3)	146[a]	1	146	258
		SH (5)	112[a]	1	112	258
Kuwae	1452	NH (2)	45[b]	1	45	138
		SH (7)	93[b]	1	93	138
Laki	1783	NH (24)	164	0.57	93	N/A[c]
Unknown	1809	NH (11)	28	1	28	54
		SH (17)	26	1	26	54
Tambora	1815	NH (22)	59	1	59	108
		SH (17)	51	1	51	108
Krakatau	1883	NH (7)	11	1	11	22
		SH (18)	11	1	11	22
Katmai	1912	NH (6)	19	0.57	11	N/A
Agung	1963	SH (17)	11	1	11	17[d]
Pinatubo	1991	SH (10)	15	1	15	30

[a]The original deposition in the Greenland and Antarctic ice sheets was multiplied by 1.13 and 1.27, respectively, to account for the spatial variation. The multipliers were calculated by comparing the average deposition of the total 7 Northern Hemisphere and 17 Southern Hemisphere ice cores to those of the 3 Northern Hemisphere and 7 Southern Hemisphere cores that have the 1259 Unknown signal.

[b]The original deposition in Greenland and Antarctic ice sheet was multiplied by 1.81 and 1.02, respectively. See *Gao et al.* [2006] for details.

[c]N/A means not applicable.

[d]We found a large signal (about 7 kg/km^2) in the Greenland ice cores during 1963–1964, but this is probably due to the aerosol input from a high-latitude NH eruption (Surtsey in Iceland). Since observations show that two thirds of the aerosols were dispersed into the SH, we can calculate the global mass loading by multiply the SH loading by 1.5 to get the total 17 Tg of aerosols.

Greenland mean deposition for Tambora. Similarly for Antarctic ice cores, we first calculated the local average deposition for the SP2001c1, SP95, PS1, PS14 cores at the South Pole; Siple Station, ITASE015, ITASE013 in the central Antarctic Peninsula; and ITASE001, ITASE991, ITASE004, ITASE005 in the western Antarctic Peninsula; respectively; before calculating the Antarctic means. The resulting Arctic and Antarctic mean sulfate deposition for the above nine eruptions, together with the number of ice cores available, are listed in columns 3 and 4 of Table 2. The deposition for 1259 Unknown and Kuwae eruption is adjusted (see Table 2 footnotes) to account for the reduction of ice cores available during those periods.

4.2. Calculation of the Calibration Factors for Tropical Eruptions

[18] Figure 8 shows the spatial distribution of total β activity (from ^{90}Sr + ^{137}Cs) from the 1952–1954 low NH latitude (11°N, LNL) and 1961–1962 high NH latitude (75°N, HNL) bomb tests in the Greenland ice sheet. Comparing Figure 8 with Figures 1 and 2, we can see that the two data sets have similar spatial coverage, though they were collected from different ice cores. The pattern of total β activity in general resembles the distribution pattern of volcanic sulfate aerosols, with large deposition near 70°N and small deposition in northeast Greenland. This confirms the previous assumption that the transport and deposition of bomb test debris resemble those of volcanic aerosols on a large scale. It also verifies, to a certain degree, the reliability of using bomb test–derived factors to estimate stratospheric sulfate loadings. *Clausen and Hammer* [1988] used the total atmospheric fission injections from USA and USSR bomb tests taken from *UNSCEAR* [1982] and calculated the calibration factor (L_B = the total β activity injected into the atmosphere by the bomb tests/the total β activity measured in Greenland ice cores) to calculate the global volcanic aerosol loadings for seven individual Greenland ice cores. Here we recalculate the factor by using the stratospheric-partitioned fission yields from the most up-to-date report [*UNSCEAR*, 2000]. We only use the stratospheric portion of the fission yields because we are interested in estimating the volcanic sulfate loading in the stratosphere. The procedures for calculating the factors include: (1) calculate the stratospheric partitioned total fission yields (*TFY*) for the 1952–1954 LNL bomb tests and 1961–1962 HNL tests separately on the basis of Table 1 of *UNSCEAR* [2000]; (2) calculate the corresponding total β activity (*TBA*) by multiplying *TFY* with sum of the production rates of ^{90}Sr (0.105 MCi of *TBA*/Mt of *TFY*) and ^{137}Cs (0.159 MCi of *TBA*/Mt of *TFY*), and (3) calculate L by dividing the *TBA* obtained in step 2 by the average *TBA* measured in ice cores in Table 2 of *Clausen and Hammer* [1988]. The value for each step is listed in Table 3. The factor is 1.51×10^9 km^2 for the 1952–1954 LNL bomb tests and 1.22×10^9 km^2 for the HNL ones. The values are much smaller than those derived by *Clausen and Hammer* [1988] for the LNL tests, but almost the same for the HNL tests. The reason is that only about 50% of the fission produced by the LNL tests was in the stratosphere whereas more than 90% of the fission produced by the HNL tests end up in the stratosphere at polar latitudes [*UNSCEAR*, 2000, Table 4].

[19] In the SH the total β activity from only three ice cores was measured by *Clausen and Hammer* [1988], which is too few to give a reliable estimate of a calibration factor given the large spatial variation in the Antarctic ice cores. However, since we have nine Antarctic ice cores that have Pinatubo signals, Law Dome, DML-B32, ITASE015, ITASE005, ITASE004, ITASE013, ITASE001, ITASE991, and SP2001c1, we can use these ice core records and satellite observations of Pinatubo sulfate aerosol loading to derive a calibration factor (L_P = the total sulfate aerosol

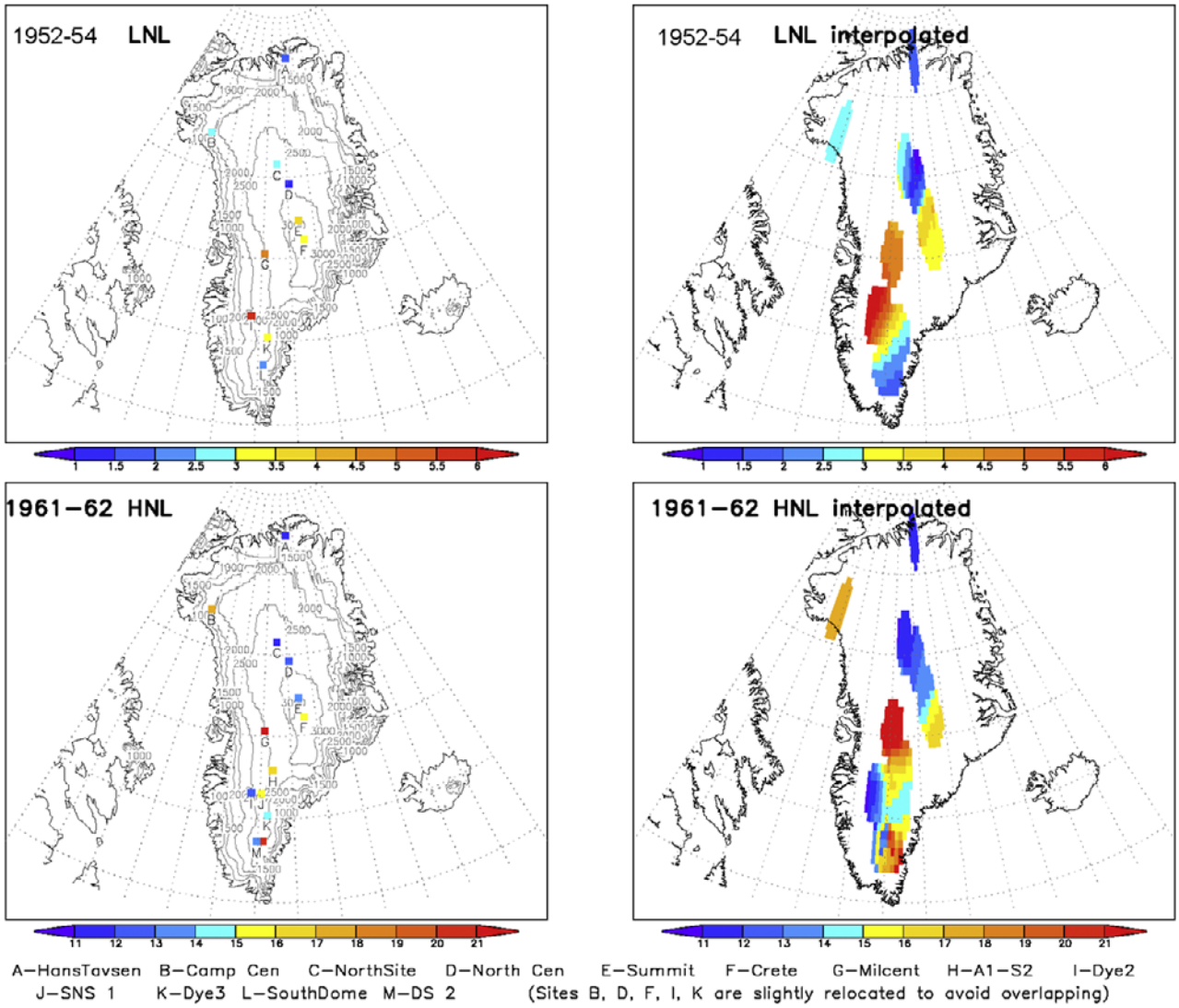

Figure 8. Spatial distribution of the total β activities from the 1952–1954 LNL and 1961–1962 HNL bomb tests.

injected into the atmosphere by Pinatubo/the average sulfate deposition measured in Antarctic ice cores) to calculate the global volcanic aerosol loadings for Antarctic ice cores. Previous studies [e.g., *Krueger et al.*, 1995] found that Pinatubo injected 15–20 Mt of SO_2 gas into the middle stratosphere. Assuming 75% H_2SO_4:25% H_2O weight composition [*Toon and Pollack*, 1973] and a complete conversion of SO_2 to H_2SO_4 aerosols, this amount of SO_2 would produce 30–40 Mt of sulfate aerosol in the stratosphere. On the other hand, the average Pinatubo sulfate deposition derived from the above nine Antarctic ice cores is 14.8 kg/km^2, which gives L_P ranging from 2.0×10^9 km^2 to 2.7×10^9 km^2.

[20] The above calibration factors were calculated on the basis of information derived from a single to a few events occurring at one latitude and altitude band under certain weather conditions, whereas the distribution of volcanic debris may differ significantly depending on the timing,

Table 3. Calculation of Stratospheric Partitioning of Total β Activity and the Calibration Factors[a]

Years of β Deposition	Stratospheric Partitioning of Total Fission Yield, Mt[b]	Total β Activity Injected in the Stratosphere, MCi[c]	Average Total β Activity in Greenland Ice Cores, mCi/km^2[d]	Calibration Factor L_B for Greenland Ice Core Records, $\times 10^9$ km^2
1952–1954 (LNL)	18.11	4.78	3.17	1.51
1961–1962 (HNL)	69.64	18.39	15.08	1.22

[a]LNL is low Northern Hemisphere latitude and HNL is high Northern Hemisphere latitude.
[b]From *UNSCEAR* [2000, Table 1].
[c]By applying the production rate of ^{90}Sr and ^{137}Cs of 0.105 MCi/Mt and 0.159 MCi/Mt.
[d]From *Clausen and Hammer* [1988, Table 2].

latitude and altitude of the volcanic injection, and the natural synoptic variability. For example, observations found that although the 1982 El Chichón (17°N) and 1991 Pinatubo (15°N) eruptions were only two degrees in latitude apart, the volcanic cloud was confined mostly to north of the Equator for the former while almost evenly distributed north and south of the Equator for the latter eruption [*Robock*, 2000]. For eruptions in the SH, the 1883 Krakatau eruption (6°S) had more or less symmetric deposition of sulfate aerosols and the 1963 Agung eruption (8°S) dispersed most of its aerosols in the SH. *Gao et al.* [2006] found that the 1452 or 1453 Kuwae eruption (17°S) also deposited about twice as much aerosol in the SH as in the NH. Therefore we propose that the low-latitude eruptions tend to disperse half to two thirds of the aerosols in the hemisphere where the eruptions take place depending on the particular distribution of the winds. With this assumption we can estimate a range of calibration factors on the basis of Greenland and Antarctic ice core records, respectively, for low-latitude eruptions with different hemispheric partitioning. For Antarctic ice core records, since our calculations indicate that the average deposition of these nine ice core records with a Pinatubo signal is very close to that from the total 19 Antarctic cores for all of the four earlier tropical eruptions (i.e., the 1809 Unknown, Tambora, Krakatau, and Agung), and satellite observations showed a relatively even distribution of the Pinatubo clouds between NH and SH, it is reasonable to assume that the Pinatubo observation–derived factor (L_P = 2.0–2.7 × 10^9 km^2) gives a fair representation of the calibration factor for tropical explosive eruptions with symmetric distribution. For eruptions that disperse two thirds of the aerosols in the SH L_P becomes 1.5–2.0 × 10^9 km^2; and for eruptions that have one third of the deposition in the SH L_P is 2.7–3.6 × 10^9 km^2. For Greenland ice core records, if we assume the bomb test debris had a symmetric distribution, L_B is 1.5 × 10^9 km^2 for eruptions with even hemispheric partitioning and 1.1 × 10^9 km^2 or 2.0 × 10^9 km^2 for eruptions that disperse two thirds or one third of the aerosols in the NH, respectively. On the other hand, if we assume the bomb test debris had a 2:1 NH:SH distribution, then L_B becomes 2.0 × 10^9 km^2 for eruptions with even hemispheric partitioning and either 1.5 × 10^9 km^2 or 3.0 × 10^9 km^2 for eruptions that disperse two thirds or one third of the aerosols in the NH correspondingly. Therefore, when using volcanic deposition calculated from Greenland ice core records, we obtained L_B ranges of 1.1–1.5 × 10^9 km^2 for eruptions that disperse two thirds of the aerosols in the NH, of 1.5–2.0 × 10^9 km^2 for eruptions with symmetric distribution, and of 2.0–3.0 × 10^9 km^2 for eruptions that disperse one third of the aerosols in the NH. Since the LNL bomb tests took place at 11°N and were more likely to disperse more debris into the NH, the calibration factor from the high end may give more accurate estimations of the actual loadings.

[21] The above calculations point to a mean calibration factor ($\overline{L}$) of about 2 × 10^9 km^2 ± 1 × 10^9 km^2 to be applied to deposition in each ice sheet to estimate the global aerosol loading for tropical eruptions. The uncertainty is about 50% of the mean value, which accounts mostly for the different hemispheric portioning of the volcanic debris and in part for the uncertainty in the satellite measurement of Pinatubo atmospheric loading. If we apply half of the value ($\overline{L}_{1/2}$ = 1 × 10^9 km^2) to the average sulfate deposition in Greenland and Antarctica separately to calculate the loading in each hemisphere and add the two hemispheric loadings to obtain the global atmospheric loading, it is not necessary to know a priori what the hemispheric partitioning was of the initial aerosol cloud, and the ice core data will reflect the actual atmospheric loading. In this way, the uncertainty may be reduced. This assumes that removal and transport processes are on the average the same in each hemisphere, but this assumption requires further investigation with detailed validated models and observations.

[22] The GISS ModelE simulation of the 1991 Pinatubo eruption produced an average sulfate deposition of 38.4 kg/km^2 over Antarctica and 42.6 kg/km^2 over Greenland. These two average values were calculated from an area-weighted average from 70°S to the South Pole and for 66°N–82°N, 50°W–35°W, respectively. The model simulation converted 20 Mt of SO_2 gas into a sulfate aerosol yield of 36 Mt by assuming a 75 wt% H_2SO_4 and 25 wt% H_2O composition. This gives a calibration factor (L_{GISS} = the global sulfate aerosol yield in the model/the Greenland or Antarctic average sulfate deposition simulated in the model) of 0.94 × 10^9 km^2 and 0.85 × 10^9 km^2 for determining the sulfate aerosol yield from Antarctica and Greenland sulfate deposition for tropical eruptions, respectively. In the simulation of the 1815 Tambora eruption, 55 Mt of SO_2 gas was injected into the 24–32 km layer which was converted into 107 Mt of sulfate aerosols. The model produced average deposition of 113.3 kg/km^2 and 78.4 kg/km^2 over the same areas in Antarctica and Greenland as for the Pinatubo eruption. Therefore L_{GISS} is 0.94 × 10^9 km^2 and 1.36 × 10^9 km^2 correspondingly. The hemispheric difference in the average deposition, and thus the calibration factors, is caused by the model's hemispheric partitioning of the aerosol (64% in NH and 36% in SH for Pinatubo and 35% in NH and 65% in SH for Tambora). Accounting for the effect of hemispheric partitioning, we obtained the global mean calibration factor ($\overline{L}_{GISS}$) as 0.91 × 10^9 km^2 and 1.09 × 10^9 km^2 for Pinatubo and Tambora, respectively.

4.3. Calculation of the Calibration Factors for High-Latitude Eruptions

[23] Two high-latitude simulations, for the 1912 Katmai and the 1783–1784 Laki eruptions, were conducted using the same model. For Katmai, 5 Mt of SO_2 gas was converted to 9.3 Mt of sulfate aerosol and the model produced an average sulfate deposition of 17 kg/km^2 over the same area of Greenland as described for Pinatubo. Therefore L_{GISS} of 0.55 × 10^9 km^2 was derived for estimating the total Katmai atmospheric loading on the basis of sulfate deposition in Greenland. A similar calibration factor was calculated for Laki. The Laki eruption was simulated using the SO_2 emission estimate from *Thordarson and Self* [2003], in which a total of 122 Mt of SO_2 gas was injected over an 8 month period with approximately 80% going into the upper troposphere/lower stratosphere. Model simulations produce a total sulfate aerosol yield of 165 Mt over the entire eruption. The average sulfate deposition over Greenland was 284 kg/km^2, gives L_{GISS} as 0.58 × 10^9 km^2. This value is very close to what we derived from Katmai even though the two eruptions are very different in both the

Table 4. Calibration Factors Derived From Three Different Methods

Method	For Tropical Eruptions Based on NH Ice Cores, $\times 10^9$ km^2			For Tropical Eruptions Based on SH Ice Cores, $\times 10^9$ km^2			
	2:1NH Versus SH	1:1NH Versus SH	1:2NH Versus SH	2:1SH Versus NH	1:1SH Versus NH	1:2SH Versus NH	For NH High-Latitude Eruptions Based on NH Ice Cores, $\times 10^9$ km^2
Bomb test calculation (L_B)	1.1–1.5	1.5–2.0	2.0–3.0	N/A[a]	N/A	N/A	1.22
Pinatubo observations (L_P)	N/A	N/A	N/A	1.5–2.0	2.0–2.7	2.7–3.6	N/A
Climate model simulations (L_{GISS})							
Tambora	N/A	N/A	1.36	0.94	N/A	N/A	N/A
Pinatubo	0.85	N/A	N/A	N/A	N/A	0.94	N/A
Laki	N/A	N/A	N/A	N/A	N/A	N/A	0.58
Katmai	N/A	N/A	N/A	N/A	N/A	N/A	0.55

[a]N/A means not available.

duration and height of gas injection and the relative distance from Greenland. *Stevenson et al.* [2003] also simulated the atmospheric loading and sulfate deposition of the Laki aerosols using specified modern atmospheric circulation coupled to a chemistry model, but their emission assumptions resulted in about 70% of the SO_2 being directly deposited to the surface before being oxidized to sulfate aerosol. As a consequence, both the lifetime and the total atmospheric loading of the sulfate aerosols were substantially smaller than those from our estimates [*Oman et al.*, 2006] and petrology estimates [*Thordarson and Self*, 2003]. Figure 7 shows that the model produced similar spatial deposition patterns for Laki and Katmai, as well as the two tropical eruptions. Thus we conclude that most Laki sulfate aerosols circulated around the Arctic with the polar vortex before being deposited on the Greenland ice sheet. Since the Laki and Katmai eruptions represent the breadth of different types of NH high-latitude eruptions it is reasonable to assume that the average calibration factor of the two events (0.57×10^9 km^2) is applicable to all NH high-latitude eruptions.

4.4. Estimates of Stratospheric Volcanic Aerosol Loadings

[24] Table 4 summarizes the calibration factors calculated from the above three methods, from which we find that the model-derived factors are substantially smaller than those from the other two methods. For tropical eruptions, it is very likely that the model underestimates the factors by up to 50% because of the faster than observed transport of volcanic aerosols from tropical eruptions which resulted in a greater sulfate deposition in high latitudes. The bomb test calculation and Pinatubo observation derived factors may thus provide better estimates of the stratospheric mass loading of the tropical eruptions. No matter what method was used, the resulting calibration factor is significantly larger than the total area of the Earth (0.51×10^9 km^2). Our model simulations (Figure 9) suggest that this is because most of the deposition is in the midlatitudes (30°–60°) in each hemisphere.

[25] For the NH high-latitude eruptions, since we have no candidate eruption that has both satellite observations and an ice core sulfate record, we cannot derive a calibration factor as we did for Pinatubo. The bomb test calculation is also not a reliable method because most HNL bomb tests were conducted in Novaya Zemlya (75°N, 60°E), 11°–17° north of where the Laki (64°N) and Katmai (58°N) eruptions took place, as well as 8° north of the Arctic Circle. Therefore the transport and deposition of the nuclear debris may not be a good model for that from lower-latitude volcanic eruptions. In addition, the HNL bomb tests were characterized by near instantaneous release of volatiles to heights larger than 20 km, whereas Laki in particular featured an eight-month-long eruption with 13–14 km high plumes and the atmospheric mass loading was confined to the low stratosphere and troposphere [*Thordarson et al.*, 1993; *Thordarson and Self*, 2003; *Fiacco et al.*, 1994]. Since both the atmospheric circulation and lifetime of aerosols are fundamentally different for the stratosphere and troposphere [*Holton et al.*, 1995], the HNL bomb tests likely misrepresent the transport and deposition of NH high-latitude volcanic aerosols. Model simulations of the Laki and Katmai eruption, on the other hand, were found to give reasonable estimates of the transport and dispersal of the aerosols [*Oman et al.*, 2006].

[26] According to the previous discussion, we decided to combine the bomb test calculation and Pinatubo observation derived factors to calculate the stratospheric sulfate aerosol loadings for tropical eruptions, while using the model-derived calibration factors to calculate the stratospheric sulfate aerosol loadings for high-latitude eruptions. Specifically for the tropical eruptions we applied $\overline{L}_{1/2} = 1.0 \times 10^9$ km^2 to the Greenland and Antarctic average deposition separately to calibrate the loadings for the corresponding hemisphere, then added the loadings calculated from each hemisphere to give the final estimate of the global loadings; for NH high-latitude eruptions we applied $\overline{L}_{GISS} = 0.57 \times 10^9$ km^2 to the average deposition in Greenland ice cores and obtained the NH aerosol loading which also stands for the global loading. Table 2 lists the atmospheric sulfate loadings of the largest eruptions during the past 1000 years obtained in this way.

[27] As shown in Table 2 we estimated the stratospheric loading of Tambora sulfate aerosols to be 108 Tg. This value is very close to the estimation of 93–118 Tg on the basis of a petrology study [*Self et al.*, 2004] but substantially smaller than the estimation of ~200 Tg by *Stothers*

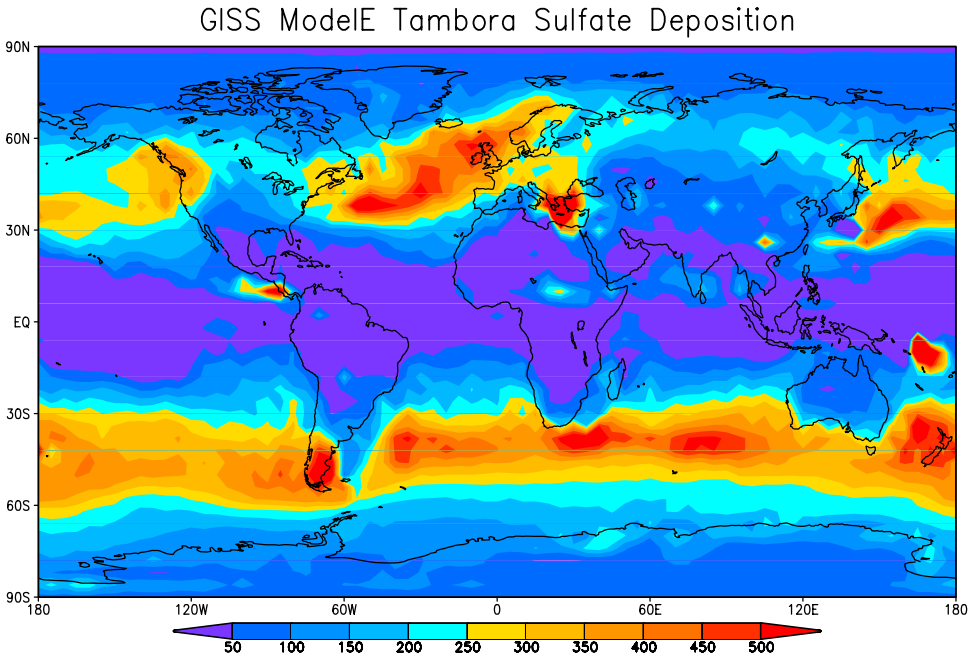

Figure 9. Global spatial distribution of the volcanic sulfate deposition (kg/km^2) after the 1815 Tambora eruption, simulated by GISS ModelE. Here 55 Mt of SO_2 gas was put into the 24–32 km layer, which converted into 107 Mt of sulfate aerosols assuming a 75%:25% H_2SO_4:H_2O weight composition.

[1984]. The latter is probably overestimated because of a local dense region of stratospheric aerosols [*Self et al.*, 2004]. The stratospheric loading of Laki is 93 Tg of sulfate aerosols, which is smaller than the estimates based on radiation (200 Mt) [*Stothers*, 1996] and geology (200 Mt) [*Thordarson and Self*, 2003], the second of which was used as input for the climate model simulation of *Oman et al.* [2006]. This is because we only estimated the stratosphere loading while the other two studies reported the total atmospheric loading instead of the stratospheric component. Observational studies [*Thordarson et al.*, 1993; *Fiacco et al.*, 1994] found that about one third to one half of the emissions from Laki were injected into the stratosphere. Thus if we multiply our estimates of Laki loading by a factor of two, this would give a total atmospheric loading of 186 Mt which is in line with other estimates. Our estimates for the rest of the eruptions (e.g., the total stratospheric sulfate aerosol loading of 30 Tg from Pinatubo, 17 Tg from Agung, and 11 Tg from Katmai) agree well with other independent studies (30 ± 10 Tg from Pinatubo [*McCormick and Veiga*, 1992; *Bluth et al.*, 1993; *McPeters*, 1995], 15 ± 5 Tg from Agung [*Rampino and Self*, 1984; *Kent and McCormick*, 1988; *Self and King*, 1996], and 11 Tg from Katmai [*Stothers*, 1996], respectively). Our estimate of stratospheric sulfate aerosol loading from Krakatau (22 Tg) is relatively smaller than that from the petrology (30–50 Tg by *Rampino and Self* [1982, 1984]) and radiation (44 Tg by *Stothers* [1996]) estimates.

4.5. Improvements From Previous Loadings Estimates and Remaining Uncertainties

[28] The above stratospheric volcanic mass loadings are the best estimations we could obtain with the available information, albeit imperfect. *Robock and Free* [1995] identified eight problems in using ice core records as measures of volcanic aerosol loading: (1) other sources of acid and bases; (2) other sources of sulfate; (3) dating uncertainties; (4) local volcanoes; (5) limited knowledge of the aerosol's pathway from the stratosphere to the ice; (6) stochastic nature of snowfall and dry deposition; (7) mixing due to blowing snow; (8) temperature dependence of ECM measurements. In the present study we used only the ice core sulfate records, which eliminated the first and the last problems. The signal extraction and deposition calculation methodology minimized the errors associated with problems (2) and (3); and our extended body of ice cores from both Greenland and Antarctica helped to distinguish local volcanoes from tropical ones in conjunction with the recent VEI index [*Siebert and Simkin*, 2002]. The information of the spatial distribution pattern obtained in section 3 was used to estimate and reduce the uncertainties caused by problems (6) and (7). The remaining challenge is to find out the relationship between atmospheric aerosol loadings and the amount of sulfate deposited in the snow and ice we were measuring. While the distribution of volcanic debris differs significantly depending on the latitude, altitude, timing of the eruption and the direction of the winds when the eruption took place, the calibration factors used in this study were derived from a single to a few events occurring at one latitude and altitude band under certain weather conditions. To account for this limitation, we calculated L_B and L_P under different assumptions of hemispheric partitioning and estimated the uncertainty range for the mean calibration factor $\overline{L}$. Simultaneous use of ice core records from both poles tells something about the hemispheric partitioning of volcanic clouds and thus would be an optimal way to estimate the global loadings. However, fewer ice core observations are available as one goes back in time to give a reliable indication of the hemispheric

partitioning as well as the magnitude of the atmospheric mass loading. Therefore proper adjustments are needed when using few ice cores to estimate strength of the earlier eruptions or the results should be interpreted with caution.

[29] Furthermore, the bomb test calculation and Pinatubo observation–derived factors are only for NH and SH respectively, because of the limited radioactivity and Pinatubo deposition measurements. The inconsistence of calibration methods may have introduced certain uncertainties in the estimation. Besides, calibration against a well-known eruption requires a linear relationship between the sulfate emitted into the stratosphere and the sulfate recovered from the ice core measurement. The linear relationship does not always hold, especially for the large eruptions.

[30] Our state-of-the-art climate model produces twice the ice core deposition as observations from both Tambora and Pinatubo, and hence the calibration factor is about half that derived from observations, assuming the model used the correct atmospheric injections of SO_2, but the model was not developed for this purpose. The general pattern of sulfate deposition shown in Figure 9, seems reasonable, but a model with much more accurate and detailed stratospheric circulation and stratospheric-tropospheric exchange needs to be developed and applied to this problem. Such a model should include high-resolution tropospheric components over the ice sheets to accurately simulate the dry and wet deposition processed there, including the detailed effects of orography.

5. Conclusion

[31] We have used 44 ice core records, 24 from Greenland, Mt. Logan, and 19 from Antarctica, and GISS ModelE simulations to examine the spatial distribution of the volcanic sulfate aerosol in the polar ice sheets. The model results and ice core observations are in general agreement, both of which suggest that the distribution of volcanic sulfate aerosol follows the general precipitation pattern in both regions, indicating the important role precipitation has played in removing the stratospheric volcanic aerosols. We estimated the relative magnitude of sulfate deposition associated with individual ice cores to the Greenland or Antarctic means, and these results provide a guideline to at least qualitatively evaluate stratospheric volcanic sulfate aerosol loading based on single or a few ice core records. We found a similar spatial distribution pattern between the volcanic sulfate deposition and the bomb test fallout in the Greenland ice cores the low-latitude and high-latitude volcanic debris, which confirms the previous assumption that the transport and deposition of bomb test debris resemble those of the volcanic aerosol. We compare three techniques for estimating stratospheric aerosol loading from ice core data, radioactive deposition from nuclear bomb tests, Pinatubo sulfate deposition in eight Antarctic ice cores, and climate model simulations of volcanic sulfate transport and deposition following the 1783 Laki, 1815 Tambora, 1912 Katmai, and 1991 Pinatubo eruptions. Combining these calibration factors with the adjustments accounting for the spatial variation, we produce estimates of the stratospheric sulfate aerosol loadings for large volcanic events during the past millennia. The results lie in the middle of the estimations based on petrology, radiation geology, and model studies and can be used to calculate the radiative forcing for the aerosol clouds and effects of these volcanic eruptions on climate.

[32] **Acknowledgments.** We thank all the scientists who have supplied us with ice core records both for the difficult work of obtaining and analyzing the cores and for allowing us to use them. We also thank two reviewers for helping us clarify our presentation. This work is supported by NOAA grant NA03-OAR-4310155, NASA grant NNG05GB06G, and NSF grants ATM-0313592 and ATM-0351280. Model development and computer time at GISS was supported by NASA climate modeling grants.

References

Bigler, M., D. Wagenbach, H. Fischer, J. Kipfstuhl, H. Millar, S. Sommer, and B. Stauffer (2002), Sulphate record from a northeast Greenland ice core over the last 1200 years based on continuous flow analysis, *Ann. Glaciol.*, *35*, 250–256.

Bluth, G. J. S., C. C. Schnetzler, A. J. Krueger, and L. S. Walter (1993), The contribution of explosive volcanism to global atmospheric sulphur dioxide concentrations, *Nature*, *366*, 327–329.

Box, J. E., D. H. Bromwich, and L. S. Bai (2004), Greenland ice sheet surface mass balance 1991–2000: Application of Polar MM5 mesoscale model and in situ data, *J. Geophys. Res.*, *109*, D16105, doi:10.1029/2003JD004451.

Bromwich, D. H., Z. C. Guo, L. S. Bai, and Q. S. Chen (2004), Modeled Antarctic precipitation. part I: Spatial and temporal variability, *J. Clim.*, *17*, 427–447.

Budner, D., and J. H. Cole-Dai (2003), The number and magnitude of large explosive volcanic eruptions between 904 and 1865 A.D.: Quantitative evidence from a new south pole ice core, in *Volcanism and the Earth*'s *Atmosphere*, *Geophys. Monogr. Ser.*, vol. 139, edited by A. Robock and C. Oppenheimer, pp. 165–176, AGU, Washington, D. C.

Clausen, H. B., and C. U. Hammer (1988), The Laki and Tambora eruptions as revealed in Greenland ice cores from 11 locations, *Ann. Glaciol.*, *10*, 16–22.

Clausen, H. B., N. S. Gundestrup, S. J. Johnsen, R. Bindschadler, and J. Zwally (1988), Glaciological investigations in the Crête area, central Greenland: A research for a new deep-drilling site, *Ann. Glaciol.*, *10*, 10–15.

Clausen, H. B., C. U. Hammer, C. S. Hvidberg, D. Dahl-Jensen, J. P. Steffensen, J. Kipfstuhl, and M. Legrand (1997), A comparison of the volcanic records over the past 4000 years from the Greenland Ice Core Project and Dye 3 Greenland Ice Cores, *J. Geophys. Res.*, *102*, 26,707–26,723.

Cole-Dai, J. H., and E. Mosley-Thompson (1999), The Pinatubo eruption in South Pole snow and its potential value to ice core paleovolcanic records, *Ann. Glaciol.*, *29*, 99–105.

Cole-Dai, J. H., E. Mosley-Thompson, and L. Thomason (1997), Annually resolved Southern Hemisphere volcanic history from two Antarctic ice cores, *J. Geophys. Res.*, *102*, 16,761–16,771.

Cole-Dai, J. H., E. Mosley-Thompson, S. P. Wight, and L. Thomason (2000), A 4100-year record of explosive volcanism from an East Antarctica ice core, *J. Geophys. Res.*, *105*, 24,431–24,441.

Cressman, G. (1959), An operational objective analysis scheme, *Mon. Weather Rev.*, *87*, 367–374.

Crowley, T. J. (2000), Causes of climate change over the past 1000 years, *Science*, *289*, 270–277.

Delmas, R. J., S. Kirchner, J. M. Palais, and J. R. Petit (1992), 1000 years of explosive volcanism recorded at the South-Pole, *Tellus, Ser. B*, *44*, 335–350.

Dixon, D., P. A. Mayewski, S. Kaspari, S. Sneed, and M. Handley (2004), A 200 year sub-annual record of sulfate in West Antarctica, from 16 ice cores, *Ann. Glaciol.*, *39*, 1–12.

Fiacco, R. J., T. Thordarson, M. S. Germani, S. Self, J. M. Palais, S. Whitlow, and P. M. Grootes (1994), Atmospheric aerosol loading and transport due to the 1783–84 Laki eruption in Iceland, interpreted from ash particles and sulfate aerosolsity in the GISP2 ice core, *Quat. Res.*, *42*, 231–240.

Free, M., and A. Robock (1999), Global warming in the context of the Little Ice Age, *J. Geophys. Res.*, *104*, 19,057–19,070.

Gao, C., A. Robock, S. Self, J. Witter, J. P. Steffenson, H. B. Clausen, M.-L. Siggaard-Andersen, S. Johnsen, P. A. Mayewski, and C. Ammann (2006), The 1452 or 1453 A.D. Kuwae eruption signal derived from multiple ice core records: Greatest volcanic sulfate event of the past 700 years, *J. Geophys. Res.*, *111*, D12107, doi:10.1029/2005JD006710.

Haynes, P., and E. Shuckburgh (2000), Effective diffusivity as a diagnostic of atmospheric transport: 1. Stratosphere, *J. Geophys. Res.*, *105*, 22,777–22,794.

Hitchman, M. H., M. McKay, and C. R. Trepte (1994), A climatology of stratospheric aerosol, *J. Geophys. Res.*, *99*, 20,689–20,700.
Holton, J. R., P. H. Haynes, M. E. Mcintyre, A. R. Douglass, R. B. Rood, and L. Pfister (1995), Stratosphere-troposphere exchange, *Rev. Geophys.*, *33*, 403–439.
Kent, G. S., and M. P. McCormick (1988), Remote sensing of stratospheric aerosol following the eruption of El Chichón, *Opt. News*, *14*, 11–19.
Krueger, A. J., L. S. Walter, P. K. Bhartia, C. C. Schnetzler, N. A. Krotkov, I. Sprod, and G. J. S. Bluth (1995), Volcanic sulfur dioxide measurements from the total ozone mapping spectrometer instruments, *J. Geophys. Res.*, *100*, 14,057–14,076.
Koch, D., G. A. Schmidt, and C. V. Field (2006), Sulfur, sea salt, and radionuclide aerosols in GISS ModelE, *J. Geophys. Res.*, *111*, D06206, doi:10.1029/2004JD005550.
Langway, C. C., H. B. Clausen, and C. U. Hammer (1988), An interhemispheric volcanic time-marker in ice cores from Greenland and Antarctica, *Ann. Glaciol.*, *10*, 102–108.
Legrand, M., and R. Delmas (1987), A 220 year continuous record of volcanic H_2SO_4 in the Antarctic ice sheet, *Nature*, *327*, 671–676.
Mayewski, P. A., W. B. Lyons, M. J. Spencer, M. S. Twickler, C. F. Buck, and S. Whitlow (1990), An ice core record of atmospheric response to anthropogenic sulfate and nitrate, *Nature*, *346*, 554–556.
Mayewski, P. A., L. D. Meeker, M. C. Morrison, M. S. Twickler, S. I. Whitlow, K. K. Ferland, D. A. Meese, M. R. Legrand, and J. P. Steffensen (1993), Greenland ice core signal characteristics: An expanded view of climate-change, *J. Geophys. Res.*, *98*, 12,839–12,847.
McCormick, M. P., and R. E. Veiga (1992), SAGE II measurements of early Pinatubo aerosols, *Geophys. Res. Lett.*, *19*, 155–158.
McPeters, R. D. (1995), Reply to the comment on the paper "The atmospheric SO_2 budget for Pinatubo derived from NOAA-11 SBUV/2 spectral data," *Geophys. Res. Lett.*, *22*, 317–320.
Moore, J. C., H. Narita, and N. Maeno (1991), A continuous 770-year record of volcanic activity from East Antarctica, *J. Geophys. Res.*, *96*, 17,353–17,359.
Mosley-Thompson, E., L. G. Thompson, J. Dai, M. Davis, and P. N. Lin (1993), Climate of the last 500 years—High-resolution ice core records, *Quat. Sci. Rev.*, *12*, 419–430.
Mosley-Thompson, E., T. A. Mashiotta, and L. G. Thompson (2003), High resolution ice core records of late Holocene volcanism: Current and future contributions from the Greenland PARCA cores, in *Volcanism and the Earth*'s *Atmosphere*, edited by A. Robock and C. Oppenheimer, pp. 153–164, AGU, Washington, D. C.
Newhall, C. G., and S. Self (1982), The volcanic explosivity index (VEI): An estimate of explosive magnitude for historical volcanism, *J. Geophys. Res.*, *87*, 1231–1238.
Oman, L., A. Robock, G. Stenchikov, T. Thordarson, D. Koch, D. Shindell, and C. Gao (2006), Modeling the distribution of the volcanic aerosol cloud from the 1783 Laki eruption, *J. Geophys. Res.*, *111*, D12209, doi:10.1029/2005JD006899.
Palmer, A. S., V. I. Morgan, A. J. Curran, T. D. Van Ommen, and P. A. Mayewski (2002), Antarctic volcanic flux ratios from Law Dome ice cores, *Ann. Glaciol.*, *35*, 329–332.
Rampino, M. R., and S. Self (1982), Historical eruptions at Tambora (1815), Krakatau (1883) and Agung (1963), their stratospheric aerosols, *Quat. Res.*, *18*, 127–143.
Rampino, M. R., and S. Self (1984), Sulphur rich volcanic eruptions and stratospheric aerosols, *Nature*, *310*, 677–679.
Reusch, D. B., P. A. Mayewski, S. I. Whitlow, I. I. Pittalwala, and M. S. Twickler (1999), Spatial variability of climate and past atmospheric circulation patterns from central West Antarctic glaciochemistry, *J. Geophys. Res.*, *104*, 5985–6001.
Robock, A. (2000), Volcanic eruptions and climate, *Rev. Geophys.*, *38*, 191–219.
Robock, A., and M. P. Free (1995), Ice cores as an index of global volcanism from 1850 to the present, *J. Geophys. Res.*, *100*, 11,549–11,567.
Robock, A., and M. P. Free (1996), The volcanic record in ice cores for the past 2000 years, in *Climatic Variations and Forcing Mechanisms of the Last 2000 Years*, edited by P. Jones et al., pp. 533–546, Springer, New York.
Sato, M., J. E. Hansen, M. P. McCormick, and J. B. Pollack (1993), Stratospheric aerosol optical depths, 1850–1990, *J. Geophys. Res.*, *98*, 22,987–22,994.
Schmidt, G. A., et al. (2006), Present day atmospheric simulations using GISS ModelE: Comparison to in-situ, satellite and reanalysis data, *J. Clim.*, *19*, 153–192.
Self, S., and A. J. King (1996), Petrology and sulfur and chlorine emissions of the 1963 eruption of Gunung Agung, Bali, Indonesia, *Bull. Volcanol.*, *58*, 263–285.
Self, S., R. Gertisser, T. Thordarson, M. R. Rampino, and J. A. Wolff (2004), Magma volume, volatile emissions, and stratospheric aerosols from the 1815 eruption of Tambora, *Geophys. Res. Lett.*, *31*, L20608, doi:10.1029/2004GL020925.
Siebert, L., and T. Simkin (2002), *Volcanoes of the World: An Illustrated Catalog of Holocene Volcanoes and their Eruptions*, *GVP-3*, Global Volcanism Program Digital Inf. Ser., Smithson. Inst., Washington, D. C. (Available at http://www.volcano.si.edu/world/.)
Stenchikov, G. L., I. Kirchner, A. Robock, H.-F. Graf, J. C. Antuña, R. G. Grainger, A. Lambert, and L. Thomason (1998), Radiative forcing from the 1991 Mount Pinatubo volcanic eruption, *J. Geophys. Res.*, *103*, 13,837–13,857.
Stenni, B., R. Caprioli, L. Cimino, C. Cremisini, O. Flora, R. Gragnani, A. Longinelli, V. Maggi, and S. Torcini (1999), 200 years of isotope and chemical records in a firn core from Hercules Névé, north Victoria Land, Antarctica, *Ann. Glaciol.*, *29*, 106–112.
Stenni, B., M. Proposito, R. Gragnani, O. Flora, J. Jouzel, S. Falourd, and M. Frezzotti (2002), Eight centuries of volcanic signal and climate change at Talos Dome (East Antarctica), *J. Geophys. Res.*, *107*(D9), 4076, doi:10.1029/2000JD000317.
Stevenson, D. S., C. E. Johnson, E. J. Highwood, V. Gauci, W. J. Collins, and R. G. Derwent (2003), Atmospheric impact of the 1783–1784 Laki eruption: Part I. Chemistry modelling, *Atmos. Chem. Phys.*, *3*, 487–507.
Stothers, R. B. (1984), The great Tambora eruption in 1815 and its aftermath, *Science*, *224*, 1191–1198.
Stothers, R. B. (1996), Major optical depth perturbations to the stratosphere from volcanic eruptions: Pyrheliometric period, 1881–1960, *J. Geophys. Res.*, *101*, 3901–3920.
Thordarson, T., and S. Self (2003), Atmospheric and environmental effects of the 1783–1784 Laki eruption: A review and reassessment, *J. Geophys. Res.*, *108*(D1), 4011, doi:10.1029/2001JD002042.
Thordarson, T., S. Self, and S. Steinthorsson (1993), Aerosol loading of the Laki fissure eruption and its impact on climate, *Eos Trans. AGU*, *74*, 106.
Toon, O. B., and J. B. Pollack (1973), Physical properties of the stratospheric aerosols, *J. Geophys. Res.*, *78*, 7051–7056.
Traufetter, F., H. Oerter, H. Fischer, R. Weller, and H. Miller (2004), Spatio-temporal variability in volcanic sulphate deposition over the past 2 kyr in snow pits and firn cores from Amundsenisen, Antarctica, *J. Glaciol.*, *50*, 137–146.
United Nations Scientific Committee on the Effects of Atomic Radiation (UNSCEAR) (1982), Ionizing radiation: Sources and biological effects, report to the General Assembly, with annexes, *U.N. Publ. E.82.IX.8*, 773 pp., New York.
United Nations Scientific Committee on the Effects of Atomic Radiation (UNSCEAR) (2000), Source and effects of ionizing radiation, report to the General Assembly, with scientific annexes, vol. 1, Sources, *U.N. Publ. E.00.IX.3,* 649 pp., New York.
Zielinski, G. A. (1995), Stratospheric loading and optical depth estimates of explosive volcanism over the last 2100 years derived from the Greenland-Ice-Sheet-Project–2 ice core, *J. Geophys. Res.*, *100*, 20,937–20,955.

C. Gao, A. Robock, and G. L. Stenchikov, Department of Environmental Sciences, Rutgers University, 14 College Farm Road, New Brunswick, NJ 08901, USA. (robock@envsci.rutgers.edu)

L. Oman, Department of Earth and Planetary Sciences, Johns Hopkins University, Olin Building, 34th and North Charles Streets, Baltimore, MD 21218, USA.